ACS OMEGA

http://pubs.acs.org/journal/acsodf

Article

Silver Nanopillar Arrayed Thin Films with Highly Surface-Enhanced Raman Scattering for Ultrasensitive Detection

Weiwei Zhang, Xiaomin Zhu, Zhanghua Chen, Vladimir I. Belotelov, and Yujun Song*

Cite This: *ACS Omega* 2022, 7, 25726−25731

Read Online

ACCESS | Metrics & More | Article Recommendations

ABSTRACT: Surface-enhanced Raman scattering (SERS) technique based on surface plasmon resonance has been considerably investigated in recent years due to its superior sensitivity in the detection of organic or biological molecules at trace levels. However, most research usually focuses on artificial architectures as SERS substrates that always have a complex and expensive micro-nanofabrication process. The high cost of masks for SERS substrates becomes a key obstacle for the widespread commercialization of SERS technology. In this paper, a biomimetic SERS substrate composed of silver-coated nanopillar arrays on the top of a cicada wing was advanced to overcome these challenges as both substrates and masks. Benefiting from the high near-field plasmon resonance coupling at the limited space among neighboring nanopillars, a dramatically increased SERS signal can be achieved using rhodamine 6G (R6G) as a model molecule. Encouragingly, the analytical enhancement factor of the order of more than 10^8 has been conveniently realized with a reliable detection concentration of R6G of about 100 pM or less. This work provides a promising route for designing cost-effective and highly sensitive SERS substrates and the related mask fabrication using our previously proposed template transfer nanoimprint.

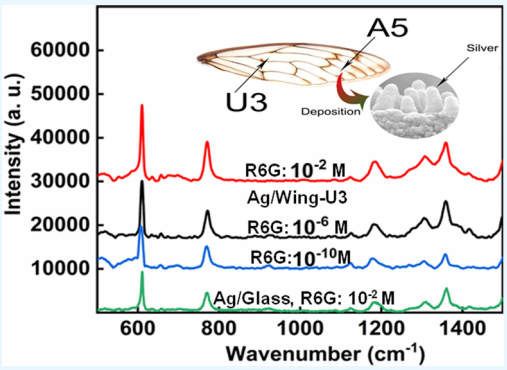

INTRODUCTION

Thanks to the real-time and ultrasensitive detection of molecules in trace amounts,[1,2] surface-enhanced Raman scattering (SERS) as an up-and-coming technique has been commonly used in various applications, including biosensors,[3−5] medicine technology,[6,7] plasmon-driven catalytic reactions,[8−16] etc. To realize these applications, as a suitable SERS substrate, there should be high-density hotspots that result from strongly enhanced electromagnetic fields caused by the localized surface plasmon resonance (LSPR).[17−22] Various types of SERS substrates have been fabricated by controllable fabrication methods to form effective hotspots, such as arrayed nanopore silver (Ag) thin films,[23] Ag-coated polymeric nanopillar arrays,[24] Ag nanoparticles assembled on a multilayer gold film by employing alumina as a spacer,[21] RGO@MoS_2@Ag ternary nanocomposites for recyclable SERS detection,[25] hydrophilic−hydrophobic Ag-modified PMMA substrates,[26] a sandwiched Ag cap nanoparticles/SiO_2/silver film system that can significantly enhance local electric-field intensity and increase the density of electromagnetic hot spots, leading to a SERS enhancement factor of 2.38×10^9,[27] and nanosculptured thin films of silver that perform a fast, accurate, and stable detection performance.[28] Additionally, the continuous metal films can also act as good electrodes for (Spectro)-electrochemistry.[29−31] However, the complex fabrication process and the cost of SERS substrates are considered as the main obstacles to the widespread commercialization of SERS spectroscopy technology.[24] In nature, many well-adapted organisms have unique and brilliant microstructures that provide a good template for research. These nanostructures can not only overcome these challenges to some extent but also exhibit substantial functionality such as droplet jumping, self-cleaning, antifogging, antimicrobial activity, and significant templates for light control.[32−37]

In this paper, a flexible and cost-effective method was proposed for the fabrication of SERS substrates. The Ag layer was directly deposited on a cicada wing using the magnetron sputtering method to form Ag-coated nanopillar SERS substrates. Benefiting from the high coupling of the electromagnetic field in the space between two adjacent nanopillars, the analytical enhancement factor (AEF) of the Ag-coated nanopillar SERS substrate for rhodamine 6G (R6G) detection can reach more than 10^8 as compared to that of the bare SERS substrate. This established relationship between the nature nanostructure and the corresponding SERS behavior provides

Received: May 15, 2022
Accepted: June 17, 2022
Published: July 11, 2022

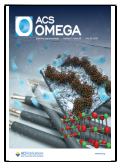

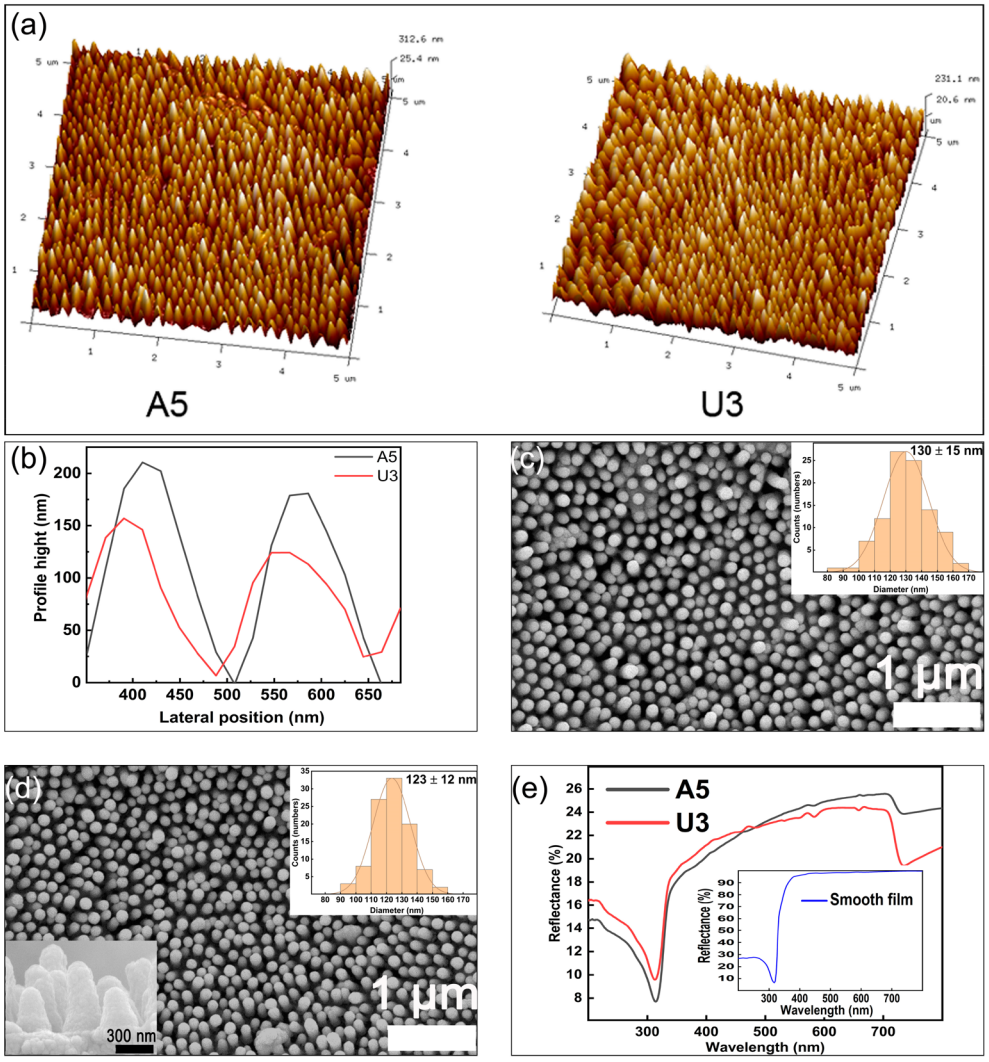

Figure 1. (a) Atomic force microscopy (AFM) scans of A5 and U3 wings. (b) Averaged AFM line scan height profiles of two adjacent nanopillars of A5 and U3 and top-viewed scanning electron microscopy images after the metal deposition for (c) A5 (the inset is the histogram of the diameter distribution of nanopillars) and (d) U3 (the insets are the high-resolution image and the histogram of the diameter distribution of nanopillars). (e) Optical reflectance spectrum of fabricated nanopillar substrates in A5 and U3 areas (the inset is the reflectance spectrum of a flat silver film as the reference).

an alternative for designing controllable platforms for biodetection applications at ultralow concentration.

RESULTS AND DISCUSSION

As shown in Figure 1a,b, biologic nanopillar cells with almost the same diameter of 50 nm at the bottom were observed on the pristine wings. The mean heights of the nanopillars on A5 and U3 samples calibrated from the three-dimensional scans were 200 and 150 nm, respectively. Here, the profiles were rezeroed based on the lowest z-coordinate when calculating the profile heights. After the magnetron sputtering process, the SEM image of the Ag-coated SERS substrate based on the A5 (Figure 1c) wing still displays a nanopillar pattern with a mean diameter of 130 nm shown in the inserted statistical image. For the U3 part, after the magnetron sputtering process, as shown in Figure 1d, it also exhibits a nanopillar pattern with a mean diameter of 123 nm, and the cross-section image inserted on the lower left corner shows that the sputtering process can form a continuous metal film on the sidewalls of the cicada wing. The optical reflectance of nanopillar substrates in A5 and U3 areas and the smooth film as reference was measured using UV−vis−NIR spectroscopy. As shown in Figure 1e, samples of A5 and U3 give a similar reflectance resonance with a dipping reflectance at 312 and 725 nm. Their reflectance increases from 350 to 700 nm. This result suggests that this kind of nanopillar thin films have higher reflectance and near-field enhancement in the optical range, which favors concentration of the energy and the surface-enhanced signals related to the reflectance and surface plasmon resonance, leading to surface-enhanced Raman scattering.[38,39]

The SERS spectra shown in Figure 2a present a comparison of SERS performances of 10^{-6} mol/L of R6G molecules adsorbed on Ag-coated nanopillars on A5 and U3 wings, Ag/glass, and pure glass substrate. There are no apparent R6G Raman peaks for the glass and Ag/glass substrates, and the standard Raman signals are negligible. However, the well-defined peaks at 610, 774, 1127, 1183, 1305, and 1361 cm^{-1} can be observed for the two types of Ag nanopillar substrates. Such peaks are attributed to C−C−C ring in-plane bending (610 cm^{-1}), C−H out-of-plane bending in the xanthene

https://doi.org/10.1021/acsomega.2c03022
ACS Omega 2022, 7, 25726−25731

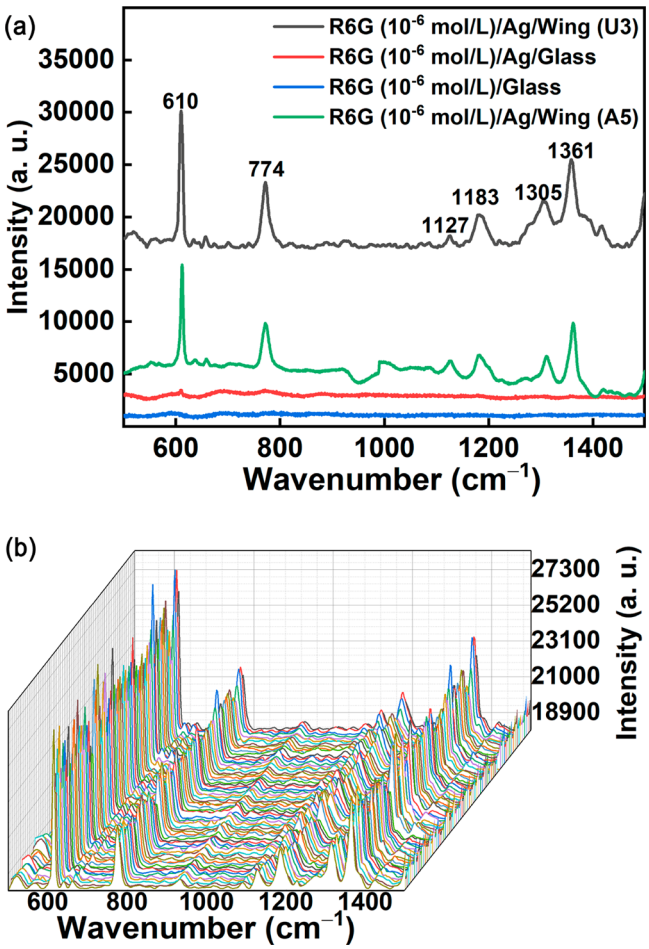

Figure 2. (a) Surface-enhanced Raman scattering spectra of 10^{-6} mol/L of R6G molecules adsorbed on Ag-coated nanopillars on A5 and U3 wings, Ag/glass, and pure glass substrates. (b) Surface-enhanced Raman scattering spectra of 10^{-6} mol/L of R6G molecules adsorbed on Ag-coated nanopillars on the U3 wing with 50 different positions.

skeleton (774 cm^{-1}), C−H in-plane bending (1127 and 1183 cm^{-1}), C−O−C stretching (1305 cm^{-1}), and aromatic C−C stretching vibrations (1361 cm^{-1}), respectively.[40−44] The SERS spectra of 10^{-6} mol/L of R6G molecules adsorbed on Ag-coated nanopillars on U3 wings with 50 different positions at a scale of 30 μm × 30 μm are shown in Figure 2b, and the calculated relative standard deviation of the intensity based on the 610 cm^{-1} is 1192, proving that the substrate exhibits good signal reproducibility and stability.

To investigate the detection limit of the Ag-coated nanopillar substrate, taking U3-based substrate as an example, the concentrations of R6G aqueous solutions varied from 10^{-2} to 10^{-10} mol/L. As shown in Figure 3, the characteristic peaks are identified in all scopes, and the peak intensity decreases distinctly with the decrease of the R6G concentration. However, even at the lowest concentration of 10^{-10} mol/L, it still demonstrates a distinguishable SERS signal.

On the basis of the adsorbed 10^{-2} mol/L of R6G aqueous solution adsorbed on the Ag/glass substrate and 10^{-10} mol/L of R6G aqueous solution adsorbed on the Ag-coated nanopillar substrate, AEF—an essential indicator of the SERS activity of a substrate—shown in eq 1 was calculated to quantify the SERS enhancement level of the fabricated Ag-coated nanopillar SERS

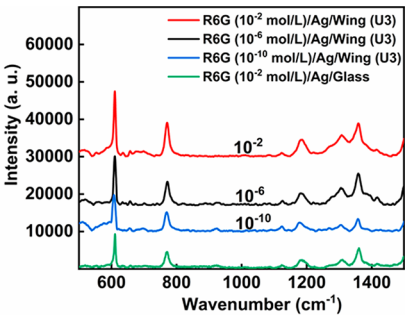

Figure 3. Surface-enhanced Raman scattering spectra (SERS) of the Ag-coated nanopillar substrate with various R6G concentrations from 10^{-2} to 10^{-10} mol/L and SERS spectrum of the Ag/glass surface with an R6G concentration of 10^{-2} mol/L.

substrate at the most intense wavenumbers 610 cm^{-1}, 774 cm^{-1}, 1183 cm^{-1}, 1313 cm^{-1}, and 1361 cm^{-1}

$$\mathrm{AEF} = (I_{\mathrm{SERS}}/C_{\mathrm{SERS}})/(I_{\mathrm{NRS}}/C_{\mathrm{NRS}}) \quad (1)$$

where C_{NAS} and C_{SERS} are the concentrations of the R6G adsorbed on the Ag/glass substrate and Ag-coated nanopillar substrate, respectively, and I_{NAS} and I_{SERS} denote the SERS intensities of R6G adsorbed on Ag/glass substrate and Ag-coated nanopillar substrate, respectively.

Two essential metrics are widely employed to quantify the overall SERS enhancement, namely, the enhancement factor (EF) and the analytical enhancement factor (AEF). EF quantifies signal enhancement by comparing SERS and the average Raman scattering signal intensity, which is a useful parameter to benchmark SERS and the moderate field enhancement experienced by each molecule across different platforms.[45,46] However, an accurate determination of the number of molecules measured within the laser excitation volume is required for this metric. Compared to the conventional enhancement factor (EF), AEF approaches signal enhancement from an analytical point of view, relating the signal intensity to the analyte concentration rather than the number of molecules. In this study, we use the AEF to describe the performance. AEF is an essential indicator of the SERS activity of a substrate and approaches signal enhancement from an analytical point-of-view, relating signal intensity to the analyte concentration rather than the number of molecules. This metric is beneficial when it is difficult to estimate the number of analyte molecules present, especially for analytes with no specific affinity for plasmonic surfaces. As summarized in Table 1, the average AEF was 8.46 × 10^7, and the AEF was up to more than 10^8 at 610 cm^{-1} and 774 cm^{-1} modes.

Table 1. Surface-Enhanced Raman Scattering Analytical Enhancement Factor (AEF) for Fabricated Ag Nanopillars

	wavenumber (cm^{-1})					
substrate	610	774	1183	1313	1361	avg AEF
Ag/U3 (10^8)	1.06	1.17	0.97	0.46	0.57	0.846

To interpret the mechanism of SERS enhancement theoretically, the electric field distribution was calculated. As shown in Figure 4a, the SEM image at a scale of 1 μm × 1 μm from the SEM image in Figure 1d was imported to COMSOL Multiphysics software to calculate the electric field distribution at a wavelength of 532 nm. In particular, consider this unit cell

https://doi.org/10.1021/acsomega.2c03022
ACS Omega 2022, 7, 25726−25731

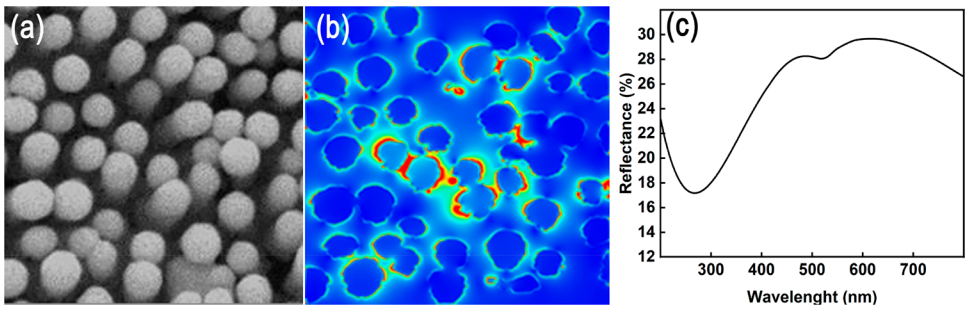

Figure 4. (a) Partial SEM image from Figure 1d with (b) its corresponding modeled electric field enhancement distributions on the top interface between the air and the sample at the excitation wavelength of 532 nm and (c) the simulated spectrum of reflectance with wavelength.

with periodic boundary conditions in the x and y directions and a perfectly matched layer in the z direction. The maximum mesh in air space is 10 nm, and mesh of the metal in the paper is 2 nm. Parts b and c, respectively, of Figure 4 show the electric field distributions on the top surface and the simulated reflectance which is basically consistent with the experimental results shown in Figure 1e. It is noticed that the intensity of the electric field tends to be stronger between two nanopillars. This indicated that the high SERS AEF observed arose predominantly from the electromagnetic enhancement induced by the plasmonic resonance coupling between adjacent Ag nanopillars.

CONCLUSION

In summary, using biomimetic nanostructures to fabricate an available SERS substrate could be considered as a flexible and cost-effective method. The Ag-coated nanopillar SERS substrate was established by directly depositing silver films on the cicada wing, giving rise to an AEF of the order of more than 10^8 in R6G detection based on the 610 cm^{-1} and 774 cm^{-1} modes due to the high near field resonance coupling of surface plasmon at the limited space among neighboring nanopillars (the mean interpillar spacing of ∼20 nm). The reliable detection concentration using rhodamine 6G as a model molecule can be 100 pM or less. These experimental results provide an alternative path to design sensitive and cost-effective SERS plasmonic sensors for the rapid and reliable detection of trace organics in biological and environmental applications.

EXPERIMENTAL METHODS

In this experiment, a cicada was first brought indoors from its habitat to complete its molt. After its natural sacrifice, without loss of generality, a central part U3, and an edge part A5, labeled according to Molds,[47] illustrated in Figure 5 were cleaned and dried for future use. Then, atomic force microscopy (AFM) was used to characterize the microstructure of the two pristine wings to determine the actual width and height using a Nanoscope V Multimode 8 scanning probe microscope (Bruker Corp.). All experiments were conducted with the same AFM probe under ambient conditions (temperature of 25 °C, the relative humidity of 25%). After the AFM imaging, a 100 nm thick Ag film was deposited on the two wings using the magnetron sputtering method at room temperature with a base pressure of 4.7×10^{-4} Pa.[48,49] During the deposition process, the metallic Ag target (purity >99.99%) was sputtered in a 15 mTorr argon gas atmosphere using a direct current sputtering apparatus with a power density of 2.5 W/cm^2.[50] Subsequently, the surface morphologies were characterized using field emission scanning electron microscopy (SEM).[23]

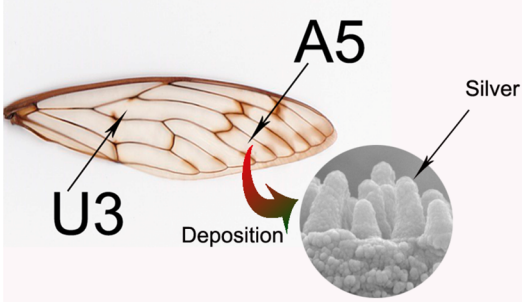

Figure 5. Photograph of the top view of the detached forewing of the cicada with two types of wing cells labeled U3 and A5 and the sliver nanorods after the deposition process.

The optical reflectance of the fabricated nanopillar substrates in A5 and U3 areas was measured by a UV−vis−NIR spectroscope (PE Lamda 750, IET Ltd.: UV−vis resolution ≤0.17 nm; NIR ≤ 0.20 nm) from 190 to 800 nm. An R6G aqueous solution was first prepared using distilled deionized water, and then the Ag-coated nanopillar SERS substrates were immersed in the R6G (BR 99.5%) solutions at concentrations of 10^{-2} mol/L, 10^{-6} mol/L, and 10^{-10} mol/L for 3 h to make R6G molecules adsorbed on the prepared substrates. To evaluate the SERS performance of the Ag-coated wing substrates, an R6G solution at a concentration of 10^{-2} mol/L adsorbed on an Ag/glass substrate was prepared as a reference. Subsequently, all of the samples were dried at room temperature. Finally, the SERS measurements were performed using an Edinburgh Raman spectrometer (RM5) under 532 nm laser irradiation with 3.4 mW of the excitation laser power, and the wavenumber was scanned from 500 cm^{-1} to 1700 cm^{-1} with a 37 s integration time.

Generally, a silver-arrayed model was used to investigate the interaction between the light and the nanostructures using the finite element method package (COMSOL Multiphysics, RF module, version 5.6) by importing the SEM image at a scale of 1 μm × 1 μm to the software. The model was illuminated by linearly polarized light along the x-axis at normal incidence, and the electric field distribution was evaluated under 532 nm laser irradiation. During the calculation, the optical constants for the silver film at the wavelength range were selected from the literature.[51] The refractive index of the environment used in the simulation was 1, since all nanostructures were immersed in the air atmosphere.

https://doi.org/10.1021/acsomega.2c03022
ACS Omega 2022, 7, 25726−25731

AUTHOR INFORMATION

Corresponding Author

Yujun Song − *Center for Modern Physics Technology, School of Mathematics and Physics, University of Science and Technology Beijing, Beijing, Haidian District, Beijing 100083, China; Zhengzhou Tianzhao Biomedical Technology Company Ltd., Zhengzhou 451450, China; Key Laboratory of Pulsed Power Translational Medicine of Zhejiang Province, Hangzhou Ruidi Biotechnology Company Ltd., Hangzhou, Zhejiang 310023, China;* orcid.org/0000-0003-2474-084X; Email: songyj@ustb.edu.cn

Authors

Weiwei Zhang − *Center for Modern Physics Technology, School of Mathematics and Physics, University of Science and Technology Beijing, Beijing, Haidian District, Beijing 100083, China; School of Mathematics and Physics, Hebei GEO University, Yuhua District, Shijiazhuang 050031, China; Shunde Graduate School, University of Science and Technology Beijing, Shunde Distinct, Foshan 528399, China*

Xiaomin Zhu − *Center for Modern Physics Technology, School of Mathematics and Physics, University of Science and Technology Beijing, Beijing, Haidian District, Beijing 100083, China*

Zhanghua Chen − *Center for Modern Physics Technology, School of Mathematics and Physics, University of Science and Technology Beijing, Beijing, Haidian District, Beijing 100083, China*

Vladimir I. Belotelov − *Vernadsky Crimean Federal University, Simferopol 295007, Russia; NTI Center for Quantum Communications, National University of Science and Technology MISiS, Moscow 119049, Russia; Photonic and Quantum Technologies School, Lomonosov Moscow State University, Leninskie Gori 119991 Moscow, Russia;* orcid.org/0000-0002-6939-4728

Complete contact information is available at: https://pubs.acs.org/10.1021/acsomega.2c03022

Notes

The authors declare no competing financial interest.

ACKNOWLEDGMENTS

This study was financially supported by BRICS STI Framework Programme by NSFC (No. 51861145309), the National Natural Science Foundation of China (No. 51971029), National S&T Major Project of China (No. 2018ZX10301201), Russian Foundation for Basic Research (Project No. 18-52-80038), the Postdoctor Research Foundation of Shunde Graduate School of University of Science and Technology Beijing (No. 2020BH005), the China Postdoctoral Science Foundation (No. 2020M680336), and the Teaching Reform Project (jgzd 20201006). V.I.B. appreciates the support from the interdisciplinary "Scientific and Educational School of Moscow University Photonic and Quantum technologies. Digital medicine. We thank Qingya Li (a scientific compass employee) from Shiyanjia Lab (www.shiyanjia.com) for the SERS test. Y.S. also appreciates the support from Zhengzhou Tianzhao Biomedical Technology Co., Ltd. (Fund No. USTB: 39080070).

REFERENCES

(1) Goel, R.; Awasthi, V.; Rai, P.; Dubey, S. K. Design of Polarization Independent SERS Substrate with Raman Gain Evaluated Using Purcell Factor. *Plasmonics* **2021**, *16* (4), 1365−1373.

(2) Huo, D.; Chen, B.; Li, M.; Meng, G.; Lei, Y.; Zhu, C. Template-assisted fabrication of Ag-nanoparticles@ZnO-nanorods array as recyclable 3D surface enhanced Raman scattering substrate for rapid detection of trace pesticides. *Nanotechnology* **2021**, *32* (14), 145302.

(3) Choi, N.; Dang, H.; Das, A.; Sim, M. S.; Chung, I. Y.; Choo, J. SERS biosensors for ultrasensitive detection of multiple biomarkers expressed in cancer cells. *Biosens Bioelectron* **2020**, *164*, 112326.

(4) Wang, M.; Li, M.; Jiang, S.; Gao, J.; Xi, P. Plasmonics meets super-resolution microscopy in biology. *Micron* **2020**, *137*, 102916.

(5) Srivastava, S. K.; Shalabney, A.; Khalaila, I.; Grüner, C.; Rauschenbach, B.; Abdulhalim, I. SERS Biosensor Using Metallic Nano-Sculptured Thin Films for the Detection of Endocrine Disrupting Compound Biomarker Vitellogenin. *Small* **2014**, *10* (17), 3579−3587.

(6) Gao, Y.; Hu, Z.; Wu, J.; Ning, Z.; Jian, J.; Zhao, T.; Liang, X.; Yang, X.; Yang, Z.; Zhao, Q.; Wang, J.; Wang, Z.; Dina, N. E.; Gherman, A. M. R.; Jiang, Z.; Zhou, H. Size-tunable Au@Ag nanoparticles for colorimetric and SERS dual-mode sensing of palmatine in traditional Chinese medicine. *J. Pharm. Biomed. Anal.* **2019**, *174*, 123−133.

(7) Lao, Z.; Zheng, Y.; Dai, Y.; Hu, Y.; Ni, J.; Ji, S.; Cai, Z.; Smith, Z. J.; Li, J.; Zhang, L.; Wu, D.; Chu, J. Nanogap Plasmonic Structures Fabricated by Switchable Capillary-Force Driven Self-Assembly for Localized Sensing of Anticancer Medicines with Microfluidic SERS. *Adv. Funct. Mater.* **2020**, *30* (15), 1909467.

(8) Cheng, Z. Q.; Li, Z. W.; Yao, R.; Xiong, K. W.; Cheng, G. L.; Zhou, Y. H.; Luo, X.; Liu, Z. M. Improved SERS Performance and Catalytic Activity of Dendritic Au/Ag Bimetallic Nanostructures Based on Ag Dendrites. *Nanoscale Res. Lett.* **2020**, *15* (1), 117.

(9) He, L.; Liu, C.; Tang, J.; Zhou, Y.; Yang, H.; Liu, R.; Hu, J. Self-catalytic stabilized Ag-Cu nanoparticles with tailored SERS response for plasmonic photocatalysis. *Appl. Surf. Sci.* **2018**, *434*, 265−272.

(10) rockia Jency, D.; Parimaladevi, R.; Arlin Jose Amali, A.; Sathe, G. V.; Umadevi, M. Colloidal design of Au@Pt nanoflowers with good catalytic activity and SERS investigations on river soil. *Colloids Surf., A* **2018**, *554*, 218−226.

(11) Li, Z.; Gao, Y.; Zhang, L.; Fang, Y.; Wang, P. Polarization-dependent surface plasmon-driven catalytic reaction on a single nanowire monitored by SERS. *Nanoscale* **2018**, *10* (39), 18720−18727.

(12) Liang, A.; Li, C.; Wang, X.; Luo, Y.; Wen, G.; Jiang, Z. Immunocontrolling Graphene Oxide Catalytic Nanogold Reaction and Its Application to SERS Quantitative Analysis. *ACS Omega* **2017**, *2* (10), 7349−7358.

(13) Nehra, K.; Pandian, S. K.; Bharati, M. S. S.; Soma, V. R. Enhanced catalytic and SERS performance of shape/size controlled anisotropic gold nanostructures. *New J. Chem.* **2019**, *43* (9), 3835−3847.

(14) Wang, P.; Liu, W.; Lin, W.; Sun, M. Plasmon-exciton co-driven surface catalytic reaction in electrochemical G-SERS. *J. Raman Spectrosc.* **2017**, *48* (9), 1144−1147.

(15) Wu, T.; Lu, Y.; Liu, J.; Zhang, S.; Zhang, X. In situ monitoring of catalytic reaction on single nanoporous gold nanowire with tuneable SERS and catalytic activity. *Talanta* **2020**, *218*, 121181.

(16) Lin, W.; Cao, E.; Zhang, L.; Xu, X.; Song, Y.; Liang, W.; Sun, M. Electrically enhanced hot hole driven oxidation catalysis at the interface of a plasmon-exciton hybrid. *Nanoscale* **2018**, *10* (12), 5482−5488.

(17) Zhang, Y. J.; Chen, S.; Radjenovic, P.; Bodappa, N.; Zhang, H.; Yang, Z. L.; Tian, Z. Q.; Li, J. F. Probing the Location of 3D Hot Spots in Gold Nanoparticle Films Using Surface-Enhanced Raman Spectroscopy. *Anal. Chem.* **2019**, *91* (8), 5316−5322.

(18) Wang, Y.; Wei, Z.; Zhang, Y.; Chen, Y. Glycerol-Assisted Construction of Long-Life Three-Dimensional Surface-Enhanced

https://doi.org/10.1021/acsomega.2c03022
ACS Omega 2022, 7, 25726−25731

Raman Scattering Hot Spot Matrix. *Langmuir* **2019**, *35* (48), 15795−15804.
(19) Li, M.; Cushing, S. K.; Zhou, G.; Wu, N. Molecular hot spots in surface-enhanced Raman scattering. *Nanoscale* **2020**, *12* (43), 22036−22041.
(20) Zhao, W.; Xiao, S.; Zhang, Y.; Pan, D.; Wen, J.; Qian, X.; Wang, D.; Cao, H.; He, W.; Quan, M.; Yang, Z. Binary "island" shaped arrays with high-density hot spots for surface-enhanced Raman scattering substrates. *Nanoscale* **2018**, *10* (29), 14220−14229.
(21) Zha, Z.; Liu, R.; Yang, W.; Li, C.; Gao, J.; Shafi, M.; Fan, X.; Li, Z.; Du, X.; Jiang, S. Surface-enhanced Raman scattering by the composite structure of Ag NP-multilayer Au films separated by Al2O3. *Opt. Express* **2021**, *29* (6), 8890−8901.
(22) Tian, Y.; Shuai, Z.; Shen, J.; Zhang, L.; Chen, S.; Song, C.; Zhao, B.; Fan, Q.; Wang, L. Plasmonic Heterodimers with Binding Site-Dependent Hot Spot for Surface-Enhanced Raman Scattering. *Small* **2018**, *14* (24), No. e1800669.
(23) Zhang, W.; Tian, Q.; Chen, Z.; Zhao, C.; Chai, H.; Wu, Q.; Li, W.; Chen, X.; Deng, Y.; Song, Y. Arrayed nanopore silver thin films for surface-enhanced Raman scattering. *RSC Adv.* **2020**, *10* (40), 23908−23915.
(24) Kim, A. N.; Lim, H.; Lee, H. N.; Park, Y. M.; Yoo, B.; Kim, H.-J. Large-area and cost-effective fabrication of Ag-coated polymeric nanopillar array for surface-enhanced Raman spectroscopy. *Appl. Surf. Sci.* **2018**, *446*, 114−121.
(25) Chen, Y.; Liu, H.; Li, X.; Tang, S.; Gu, C.; Wei, G.; Jiang, T.; Zhou, X. Development of RGO@MoS2@Ag ternary nanocomposites with tunable geometry structure for recyclable SERS detection. *Sens. Actuators, B* **2021**, *339*, 129856.
(26) Tang, S.; Liu, H.; Tian, Y.; Chen, D.; Gu, C.; Wei, G.; Jiang, T.; Zhou, J. Surface-enhanced Raman scattering-based lateral flow immunoassay mediated by hydrophilic-hydrophobic Ag-modified PMMA substrate. *Spectrochim. Acta, Part A* **2021**, *262*, 120092.
(27) Wu, H.-Y.; Cunningham, B. T. Plasmonic coupling of SiO2-Ag "post-cap" nanostructures and silver film for surface enhanced Raman scattering. *Appl. Phys. Lett.* **2011**, *98* (15), 153103.
(28) Srivastava, S. K.; Hamo, H. B.; Kushmaro, A.; Marks, R. S.; Grüner, C.; Rauschenbach, B.; Abdulhalim, I. Highly sensitive and specific detection of E. coli by a SERS nanobiosensor chip utilizing metallic nanosculptured thin films. *Analyst* **2015**, *140* (9), 3201−3209.
(29) Akinoglu, G. E.; Mir, S. H.; Gatensby, R.; Rydzek, G.; Mokarian-Tabari, P. Block Copolymer Derived Vertically Coupled Plasmonic Arrays for Surface-Enhanced Raman Spectroscopy. *ACS Appl. Mater. Interfaces* **2020**, *12* (20), 23410−23416.
(30) Viehrig, M.; Rajendran, S. T.; Sanger, K.; Schmidt, M. S.; Alstrøm, T. S.; Rindzevicius, T.; Zór, K.; Boisen, A. Quantitative SERS Assay on a Single Chip Enabled by Electrochemically Assisted Regeneration: A Method for Detection of Melamine in Milk. *Anal. Chem.* **2020**, *92* (6), 4317−4325.
(31) Akinoglu, G. E.; Hutchison, J. A. Perspective—Quasi-Babinet Complementary Plasmonic Templates: A Platform to Perform Spectroelectrochemistry. *ECS Journal of Solid State Science and Technology* **2021**, *10* (3), 035005.
(32) Stoddart, P. R.; Cadusch, P. J.; Boyce, T. M.; Erasmus, R. M.; Comins, J. D. Optical properties of chitin: surface-enhanced Raman scattering substrates based on antireflection structures on cicada wings. *Nanotechnology* **2006**, *17* (3), 680−686.
(33) Shao, F.; Lu, Z.; Liu, C.; Han, H.; Chen, K.; Li, W.; He, Q.; Peng, H.; Chen, J. Hierarchical Nanogaps within Bioscaffold Arrays as a High-Performance SERS Substrate for Animal Virus Biosensing. *ACS Appl. Mater. Interfaces* **2014**, *6* (9), 6281−6289.
(34) Sun, H.; Li, X.; Gu, C.; Zhang, J.; Wei, G.; Jiang, T.; Zhou, X. Bioinspired surface-enhanced Raman scattering substrate with intrinsic Raman signal for the interactive SERS detection of pesticides residues. *Spectrochimica Acta Part A: Molecular and Biomolecular Spectroscopy* **2022**, *270*, 120800.
(35) Rubio-Roy, M.; Vlasin, O.; Pascu, O.; Caicedo, J. M.; Schmidt, M.; Goni, A. R.; Tognalli, N. G.; Fainstein, A.; Roig, A.; Herranz, G. Magneto-optical enhancement by plasmon excitations in nanoparticle/metal structures. *Langmuir* **2012**, *28* (24), 9010−20.
(36) Luiggi, C. Color from Structure. *Scientist* **2013**, *27* (2), 42−48.
(37) Oh, J.; Dana, C. E.; Hong, S.; Roman, J. K.; Jo, K. D.; Hong, J. W.; Nguyen, J.; Cropek, D. M.; Alleyne, M.; Miljkovic, N. Exploring the Role of Habitat on the Wettability of Cicada Wings. *ACS Appl. Mater. Interfaces* **2017**, *9* (32), 27173−27184.
(38) Song, S.; Keating, M.; Chen, Y.; Placido, F. Reflectance and surface enhanced Raman scattering (SERS) of sculptured silver films deposited at various vapor incident angles. *Meas. Sci. Technol.* **2012**, *23*, 084007.
(39) Zhao, Y.; Liu, Y. The Silver Nanorod Array SERS Substrates. *AIP Conf. Proc.* **2010**, *1267* (1), 277−278.
(40) Hildebrandt, P.; Stockburger, M. Surface-Enhanced Resonance Raman Spectroscopy of Rhodamine 6G adsorbed on colloidal silver. *J. Phys. Chem.* **1984**, *88* (24), 5935−5944.
(41) Tiwari, V. S.; Oleg, T.; Darbha, G. K.; Hardy, W.; Singh, J. P.; Ray, P. C. Non-resonance SERS effects of silver colloids with different shapes. *Chem. Phys. Lett.* **2007**, *446* (1−3), 77−82.
(42) Coluccio, M. L.; Das, G.; Mecarini, F.; Gentile, F.; Pujia, A.; Bava, L.; Tallerico, R.; Candeloro, P.; Liberale, C.; Angelis, F. D. Silver-based surface enhanced Raman scattering (SERS) substrate fabrication using nanolithography and site selective electroless deposition. *Microelectron. Eng.* **2009**, *86* (4), 1085−1088.
(43) Yang, K. H.; Liu, Y. C.; Yu, C. C. Enhancements in intensity and stability of surface-enhanced Raman scattering on optimally electrochemically roughened silver substrates. *J. Mater. Chem.* **2008**, *18* (40), 4849−4855.
(44) He, S.; Xie, W.; Fang, S.; Huang, X.; Zhou, D.; Zhang, Z.; Du, J.; Du, C.; Wang, D. Silver films coated inverted cone-shaped nanopore array anodic aluminum oxide membranes for SERS analysis of trace molecular orientation. *Appl. Surf. Sci.* **2019**, *488*, 707−713.
(45) Chaney, S. B.; Shanmukh, S.; Dluhy, R. A.; Zhao, Y. P. Aligned silver nanorod arrays produce high sensitivity surface-enhanced Raman spectroscopy substrates. *Appl. Phys. Lett.* **2005**, *87* (3), 031908.
(46) Yang, Y.; Peng, Y.; Lin, C.; Long, L.; Hu, J.; He, J.; Zeng, H.; Huang, Z.; Li, Z.-Y.; Tanemura, M.; Shi, J.; Lombardi, J. R.; Luo, X. Human ACE2-Functionalized Gold "Virus-Trap" Nanostructures for Accurate Capture of SARS-CoV-2 and Single-Virus SERS Detection. *Nano-Micro Letters* **2021**, *13* (1), 109.
(47) Moulds, M. S. An Appraisal of the Higher Classification of Cicadas (Hemiptera: Cicadoidea) with Special Reference to the Australian Fauna. *Rec. Aust. Mus.* **2005**, *57* (3), 375−446.
(48) Zhang, W.; Chen, Z.; Belotelov, V. I.; Song, Y. Longitudinal Magneto-Optical Kerr Effect of Nanoporous CoFeB and W/CoFeB/W Thin Films. *Coatings* **2022**, *12* (2), 115.
(49) Zhu, X.; Zhao, C.; Zhang, W.; Zhang, B.; Sun, M.; Chen, X.; Belotelov, V. I.; Song, Y. Structural Color Control of CoFeB-Coated Nanoporous Thin Films. *Coatings* **2021**, *11* (9), 1123.
(50) Zhang, W.; Wang, Q.; Zhao, C.; Song, Y. The optical cavity enhanced magneto-optical Kerr effect signals of AAO/Al-based CoFeB nanostructure arrays. *Opt. Commun.* **2019**, *437*, 44−49.
(51) Werner, W. S. M.; Glantschnig, K.; Ambrosch-Draxl, C. Optical Constants and Inelastic Electron-Scattering Data for 17 Elemental Metals. *J. Phys. Chem. Ref. Data* **2009**, *38* (4), 1013−1092.

https://doi.org/10.1021/acsomega.2c03022
ACS Omega 2022, 7, 25726−25731